

# Physics-Informed Neural Networks for Speech Production

Kazuya Yokota *Member, IEEE*, Ryosuke Harakawa *Member, IEEE*, Masaaki Baba, and Masahiro Iwahashi *Senior Member, IEEE*

**Abstract**—The analysis of speech production based on physical models of the vocal folds and vocal tract is essential for studies on vocal-fold behavior and linguistic research. This paper proposes a speech production analysis method using physics-informed neural networks (PINNs). The networks are trained directly on the governing equations of vocal-fold vibration and vocal-tract acoustics. Vocal-fold collisions introduce nondifferentiability and vanishing gradients, challenging phenomena for PINNs. We demonstrate, however, that introducing a differentiable approximation function enables the analysis of vocal-fold vibrations within the PINN framework. The period of self-excited vocal-fold vibration is generally unknown. We show that by treating the period as a learnable network parameter, a periodic solution can be obtained. Furthermore, by implementing the coupling between glottal flow and vocal-tract acoustics as a hard constraint, glottis-tract interaction is achieved without additional loss terms. We confirmed the method’s validity through forward and inverse analyses, demonstrating that the glottal flow rate, vocal-fold vibratory state, and subglottal pressure can be simultaneously estimated from speech signals. Notably, the same network architecture can be applied to both forward and inverse analyses, highlighting the versatility of this approach. The proposed method inherits the advantages of PINNs, including mesh-free computation and the natural incorporation of nonlinearities, and thus holds promise for a wide range of applications.

**Note:** This work has been submitted to the IEEE for possible publication. Copyright may be transferred without notice, after which this version may no longer be accessible.

**Index Terms**—Speech production, physics-informed neural networks, PINNs, vocal folds, and vocal tract.

## I. INTRODUCTION

SPEECH production analysis based on physical models plays an important role in studies of vocal-fold behavior [1], [2], diagnosis of voice disorders [3], [4], and linguistics [5], [6]. Studies on the vibratory modes of the vocal folds [1], [7] and simulations predicting postsurgical changes in voice [8], [9] illustrate the importance of physical modeling in speech research. Model-based studies often attempt to estimate vocal-fold or vocal-tract states directly from speech data [10]–[12], enabling the inference of articulatory states from readily observable signals. However, many of these methods rely on the assumption of independence between the source (vocal-fold vibration) and the filter (vocal-tract acoustics) [13]. To achieve more realistic physical analyses, inverse methods that include vocal-fold dynamics are required. However, conventional solvers (e.g., finite-difference methods) are designed primarily for forward analyses and require

Kazuya Yokota and Masaaki Baba are with the Department of Mechanical Engineering, Nagaoka University of Technology, 1603-1, Kamitomioka, Nagaoka, Niigata, Japan (e-mail: yokokazu@vos.nagaokaut.ac.jp). Ryosuke Harakawa and Masahiro Iwahashi are with the Department of Electrical, Electronics and Information Engineering, Nagaoka University of Technology (e-mail: iwahashi@vos.nagaokaut.ac.jp).

dedicated algorithms for inverse analyses involving vocal-fold vibrations [14]. In addition, coupled analyses of the vocal folds and vocal tract are inherently multiphysical (structure-fluid-acoustic) problems, making the construction of such models complex. Traditional time and space discretization approaches also suffer from increased computational cost when performing detailed simulations [15].

Physics-informed neural networks (PINNs) [16] offer a promising approach to these challenges, having recently attracted attention as powerful numerical frameworks for inverse problems [17], [18]. PINNs incorporate governing equations as loss function constraints, enabling mesh-free simulation [16], natural handling of nonlinearities [19], and inverse analysis using the same network as for forward analysis [16]. PINN applications in acoustics are expanding, including acoustic admittance estimation from noisy measurements [20], acoustic impulse response reconstruction [21], and sound pressure distribution estimation [22], all demonstrating their potential for acoustic inverse problems. Nevertheless, PINN applications in speech analysis remain limited, with few reports apart from our previous work on vocal-tract acoustics [23]. Although PINNs based on physical models of speech production hold great promise for diagnosing voice disorders and for inverse mapping of articulatory mechanisms, to our knowledge, no studies have analyzed human speech production using PINNs that explicitly include vocal-fold vibrations.

Several challenges arise when applying PINNs to speech-production analysis. First, glottal flow nondifferentiability and vanishing gradients are problematic. Glottal closure during vocal-fold collision introduces points where the time derivatives are undefined [7]. Moreover, because the flow becomes zero during closure, there are intervals in which the time derivative of the glottal flow is zero. Although PINNs, according to the universal approximation theorem [24], can approximate continuous functions, these issues hinder back-propagation training [25] and degrade learning performance [26], [27]. Second, the vocal-fold self-oscillation period is generally unknown. Owing to the spectral bias of PINNs [28], [29], shorter analysis time windows enable a higher frequency resolution [30], making it desirable, similar to the shooting method [31], to analyze only a single steady-state oscillation cycle. However, the unknown period of self-oscillation prevents the prior determination of collocation points in time. Additional challenges include the multiphysics coupling between the vocal folds and vocal tract, as well as high-frequency acoustic analysis of higher formants, which complicate designing PINNs for speech production.

In this paper, we present the first PINNs for speech production to address these challenges. To handle glottal closure, we introduced differentiable approximation functions to facil-

itate stable learning. To cope with the unknown oscillation period, we treated the period as a learnable parameter of the network and introduced a time-scaling variable, enabling the automatic identification of the period without reconfiguring the collocation points. For glottal flow-vocal tract coupling, we demonstrated that implementing the interaction as a hard constraint eliminates the need for additional loss terms. As a foundational study, the Ishizaka–Flanagan two-mass model [1] was adopted for the vocal folds, and a one-dimensional acoustic model [23], [32] was used for the vocal tract. The validity of the proposed method was confirmed through both forward analysis of vowel generation and inverse analysis, estimating vocal-fold vibration states and subglottal pressure from speech waveforms. In particular, for the inverse analysis, we demonstrate that, using nearly the same network as for the forward analysis, it is possible to simultaneously estimate the glottal flow, vocal-fold vibration waveform, and subglottal pressure from the speech signal without constructing complex algorithms specifically for inversion. The contributions of this study are as follows:

- 1) The proposal of a PINN that enables speech production analysis including vocal-fold vibration.
- 2) A methodology for constructing PINNs capable of handling glottal closure, unknown oscillation periods, and coupling between glottal flow and vocal-tract acoustics.
- 3) The demonstration of the first PINN to simultaneously perform inverse estimation of glottal flow, vocal-fold vibration waveform, and subglottal pressure from a speech signal.

The remainder of this paper is organized as follows: Section II describes the governing equations of the vocal-fold and vocal-tract models. Section III introduces the PINN framework for speech production and adapts its architecture to the underlying physics. Section IV presents the forward and inverse analyses using the proposed method and validates the approach. Section V concludes the paper with a summary and discussion of the potential applications of the proposed PINNs in speech production.

## II. GOVERNING EQUATIONS OF SPEECH PRODUCTION

This section describes the governing equations of vocal-fold vibration and vocal-tract acoustics used in this study.

### A. Two-mass Model of Vocal Folds

In this study, the Ishizaka–Flanagan two-mass model [1] was used as the vocal-fold vibration model. As illustrated in Fig. 1, the vocal folds are represented by two masses, and the glottal flow is assumed to be one-dimensional, incompressible, and quasi-steady, satisfying Bernoulli's principle. Let  $u_g$  be the glottal volume flow. As shown in Fig. 1, pressure variations occur at different positions along the glottis depending on the vocal-fold shape. These variations are expressed by the following equations [1]:

$$p_{11} = p_s - R_c u_g^2, \quad (1)$$

$$p_{12} = p_{11} - R_{v1} u_g, \quad (2)$$

$$p_{21} = p_{12} - R_{12} u_g^2, \quad (3)$$

$$p_{22} = p_{21} - R_{v2} u_g, \quad (4)$$

$$p_0 = p_{22} - R_e u_g^2, \quad (5)$$

where

$$R_c = 1.37 \frac{\rho}{2A_{g1}^2}, \quad (6)$$

$$R_{v1} = 12 \frac{\mu l_g^2 d_1}{A_{g1}^3}, \quad (7)$$

$$R_{12} = \frac{\rho}{2} \left( \frac{1}{A_{g2}^2} - \frac{1}{A_{g1}^2} \right), \quad (8)$$

$$R_{v2} = 12 \frac{\mu l_g^2 d_2}{A_{g2}^3}, \quad (9)$$

$$R_e = -\frac{\rho}{A_{g2} A_0} \left( 1 - \frac{A_{g2}}{A_0} \right), \quad (10)$$

where  $p_s$  is the subglottal pressure,  $\rho$  is the air density,  $\mu$  is the viscosity of the air,  $l_g$  is the vocal-fold length in the direction perpendicular to the flow,  $d_1$  and  $d_2$  are the vocal-fold thicknesses in the flow direction,  $A_0$  is the cross-sectional area at the vocal-tract entrance, and  $p_0$  is the pressure at the vocal-tract entrance.  $A_{g1}$  and  $A_{g2}$  denote the cross-sectional areas of the flow channels, given by

$$A_{g1} = A_{g01} + 2l_g x_1 \quad \text{for } x_1 > x_{\min 1}, \quad (11)$$

$$A_{g1} = 0 \quad \text{for } x_1 \leq x_{\min 1}, \quad (12)$$

$$A_{g2} = A_{g02} + 2l_g x_2 \quad \text{for } x_2 > x_{\min 2}, \quad (13)$$

$$A_{g2} = 0 \quad \text{for } x_2 \leq x_{\min 2}, \quad (14)$$

where  $x_1$  and  $x_2$  are the displacements from the equilibrium positions of the two masses;  $x_{\min}$  is the collision position; and  $A_{g0,j} = -2l_g x_{\min,j}$ . Equation (1) represents narrowing at the glottal entrance. Equations (2) and (4) account for viscous losses. Equation (3) describes the variation in the glottal cross-sectional area, and Eq. (5) expresses the pressure recovery owing to flow separation and reattachment. Assuming that the flow is quasi-steady and that air inertia is negligible [33], [34],  $u_g$  is obtained from Eqs. (1)-(5) as follows:

$$u_g = \frac{-R_\beta + \sqrt{R_\beta^2 - 4R_\alpha R_\gamma}}{2R_\alpha}, \quad (15)$$

where

$$R_\alpha = R_c + R_{12} + R_e, \quad (16)$$

$$R_\beta = R_{v1} + R_{v2}, \quad (17)$$

$$R_\gamma = p_0 - p_s. \quad (18)$$

Vocal folds vibrate under aerodynamic pressure. The spring force is then given by:

$$s_j = k_j (x_j + \eta_{k,j} x_j^3), \quad j = 1, 2, \quad \text{for } x_j > x_{\min,j}, \quad (19)$$

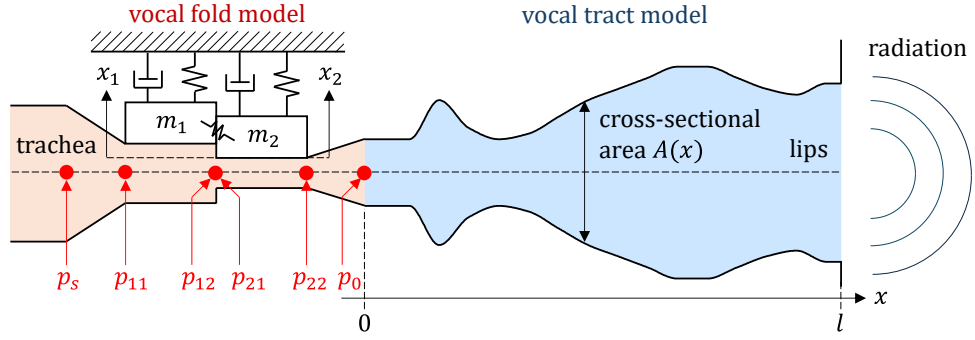


Fig. 1. Vocal-fold and vocal-tract models used in this study. The vocal folds are represented by the Ishizaka–Flanagan two-mass model [1], and the vocal tract is represented by a one-dimensional acoustic tube model [32].

where  $j$  denotes the mass index,  $k$  is the linear spring constant, and  $\eta_k$  is the nonlinear spring coefficient. When the glottis is closed, the vocal folds collide and the elastic force becomes

$$s_j = k_j (x_j + \eta_{k,j} x_j^3) + h_j \{(x_j + x_{\min,j}) + \eta_{h,j} (x_j + x_{\min,j})^3\}, \quad (20)$$

$$j = 1, 2, \quad \text{for } x_j \leq x_{\min,j},$$

where  $h$  is the linear collision spring constant and  $\eta_h$  is the nonlinear collision spring coefficient. The equations of motion of the vocal folds are as follows:

$$m_1 \ddot{x}_1 + c_1 \dot{x}_1 + s_1 + k_c (x_1 - x_2) = f_1, \quad (21)$$

$$m_2 \ddot{x}_2 + c_2 \dot{x}_2 + s_2 + k_c (x_2 - x_1) = f_2, \quad (22)$$

where  $c$  is the damping coefficient, and  $k_c$  is the coupling spring constant connecting the two masses. The external force  $f_j$  acting on the folds was computed as follows:

$$f_1 = l_g d_1 p_1, \quad f_2 = l_g d_2 p_2, \quad \text{for } x_1 > x_{\min,1}, \quad x_2 > x_{\min,2}, \quad (23)$$

$$f_1 = l_g d_1 p_s, \quad f_2 = 0, \quad \text{for } x_1 \leq x_{\min,1}, \quad x_2 > x_{\min,2}, \quad (24)$$

$$f_1 = l_g d_1 p_s, \quad f_2 = l_g d_2 p_s, \quad \text{for } x_1 > x_{\min,1}, \quad x_2 \leq x_{\min,2}, \quad (25)$$

$$f_1 = l_g d_1 p_s, \quad f_2 = 0, \quad \text{for } x_1 \leq x_{\min,1}, \quad x_2 \leq x_{\min,2}, \quad (26)$$

where

$$p_1 = (p_{11} + p_{12})/2, \quad (27)$$

$$p_2 = (p_{21} + p_{22})/2. \quad (28)$$

Vocal folds vibrate through the interaction between elasticity and glottal flow. This two-mass model is widely accepted as a fundamental representation of vocal-fold vibrations [35], [36] and is used in this study to construct the PINN framework.

### B. One-dimensional Model of Vocal Tract

In this study, a one-dimensional acoustic tube model [32] was used as the vocal-tract model. As shown in Fig. 1, with the axial position denoted by  $x$ , the vocal tract is modeled as a tube of length  $l$  with a circular cross-section of area  $A(x)$ . Let  $p$  denote the sound pressure and  $u$  be the volume velocity

inside the tract. The propagation of sound waves is expressed as follows [32]:

$$\frac{\partial u}{\partial x} = -Gp - \frac{A}{K} \frac{\partial p}{\partial t}, \quad (29)$$

$$\frac{\partial p}{\partial x} = -Ru - \frac{\rho}{A} \frac{\partial u}{\partial t}. \quad (30)$$

where  $G$  represents the energy loss due to thermal conduction at the wall,  $R$  represents the energy loss due to wall viscosity, and  $K$  is the bulk modulus. Assuming rigid walls with infinite thermal conductivity, the theoretical expressions for  $R$  and  $G$  are given by:

$$R = \alpha_R \frac{S}{A^2} \sqrt{\frac{\omega_c \rho \mu}{2}}, \quad (31)$$

$$G = \alpha_G S \frac{\eta_{\text{air}} - 1}{\rho c_{\text{air}}^2} \sqrt{\frac{\lambda_{\text{air}} \omega_c}{2 c_p \rho}}, \quad (32)$$

where  $S$  is the circumference of the acoustic tube,  $\eta_{\text{air}}$  is the specific heat ratio of air,  $c_{\text{air}}$  is the speed of sound,  $\lambda_{\text{air}}$  is the thermal conductivity of air,  $c_p$  is the specific heat at constant pressure, and  $\omega_c$  is the angular frequency used for the loss calculations. The coefficient  $\alpha_R$  is a multiplicative factor introduced by Ishizaka and Flanagan [1] to account for losses not included in the theoretical expression, whereas  $\alpha_G$  is a multiplicative factor applied to  $G$ .

As shown in Fig. 1, sound radiation from the lips is assumed at the position  $x = l$ . Assuming that the particle velocity at the open end is uniform and that the opening is surrounded by an infinite planar baffle, the relationship between the sound pressure  $p_l$  ( $p$  at  $x = l$ ) and volume velocity  $u_l$  ( $u$  at  $x = l$ ) at the open end can be expressed by the following equivalent circuit [1]:

$$(u_l - u_r) R_r = L_r \frac{du_r}{dt}, \quad (33)$$

$$p_l = (u_l - u_r) R_r, \quad (34)$$

where  $u_r$  is the virtual volume velocity introduced for the radiation calculation and  $R_r$  and  $L_r$  represent the resistance

and reactance in the equivalent circuit, respectively.  $R_r$  and  $L_r$  are calculated as follows:

$$R_r = \frac{128\rho c}{9\pi^2 A_l}, \quad (35)$$

$$L_r = \frac{8\rho}{3\pi\sqrt{\pi}A_l}, \quad (36)$$

where  $A_l$  denotes the cross-sectional area at  $x = l$ . Applying Kirchhoff's current law to Eqs. (33) and (34) yields

$$L_r \frac{du_l}{dt} = p_l + \frac{L_r}{R_r} \frac{dp_l}{dt}. \quad (37)$$

In this paper, Eq. (37) is employed as the boundary condition at the open end.

### C. Coupling of Vocal-Fold and Vocal-Tract Models

In this study, a coupled analysis of the vocal folds and tract was performed. To calculate  $u_g$  using Eq. (15), the pressure at the entrance of the vocal tract  $p_0$  is required. Therefore,  $p_0$  is set to match the pressure  $p$  at  $x = 0$  from the vocal-tract model:

$$p_0(t) = p(x, t)|_{x=0}. \quad (38)$$

To analyze acoustic wave propagation in the vocal tract based on Eqs. (29) and (30), a volume velocity waveform at  $x = 0$  is required. Accordingly, the volume velocity  $u$  at  $x = 0$  in the vocal tract is matched to the glottal volume velocity  $u_g$ :

$$u(x, t)|_{x=0} = u_g(t). \quad (39)$$

Through this coupling, the vocal folds exhibit self-excited oscillations that correspond to the resonance characteristics of the vocal tract.

## III. PROPOSED METHOD

In this section, we describe the proposed PINN architecture for speech production.

### A. Overview of PINN Architecture for Speech Production

Figure 2 illustrates the proposed PINN architecture for speech production. The proposed architecture consists of two networks: the upper network outputs the predicted values of  $x_1$  and  $x_2$ , which are the solutions to Eqs. (21) and (22), representing vocal-fold vibrations, whereas the lower network outputs  $\tilde{p}$  and  $\tilde{u}$ , which are used to predict  $p$  and  $u$ , the solutions of Eqs. (29) and (30). Each network is composed of fully connected layers, activation layers, and an FC block [37] that we employed previously. Similar to our earlier PINN framework for acoustic resonance analysis [37], the activation layers in this study use a snake function [38]. The design of each network component is illustrated in Fig. 2.

### B. Input Mapping

In this model, only one steady-state period was considered for the analysis. In the input part shown in Fig. 2,  $x$  and  $t$  are normalized to the range  $[-1, 1]$  as follows:

$$x^* = \frac{2x}{l} - 1, \quad (40)$$

$$t^* = \frac{2t}{T} - 1. \quad (41)$$

Note that  $T$  is the period; the original range of  $t$  is  $[0, T]$  and that of  $x$  is  $[0, l]$ . For  $t^*$ , the following Fourier feature mapping [39] is applied:

$$\mathbf{t}^* = \left[ \cos \frac{\pi t^*}{T}, \sin \frac{\pi t^*}{T}, \dots, \cos \frac{m\pi t^*}{T}, \sin \frac{m\pi t^*}{T} \right], \quad (42)$$

where  $m$  is the number of Fourier features. Fourier feature mapping improves the accuracy of PINNs in high-frequency region [40], [41]. Furthermore, because Eq. (42) yields identical values for  $\mathbf{t}^*$  at  $t = 0$  and  $t = T$ , periodicity can be satisfied as a hard constraint.

### C. Hard Constraint for Coupled Analysis

This section describes the method for coupling the equations for vocal-fold vibrations and vocal-tract acoustics. In conventional PINNs, the coupling of physical quantities in multiphysics problems is generally achieved through soft constraints using additional loss functions [42], [43]. However, introducing extra loss terms requires new hyperparameter tuning and increases the computational training costs. In the proposed method, glottal flow velocity  $u_g$  coupling is enforced as a hard constraint. As a preliminary step, the network output  $\tilde{p}$  of the vocal tract was processed to obtain the acoustic pressure  $p$  inside the tract:

$$p = \tilde{p} \cos \frac{\pi}{2l} x + p_{\text{data}} \left( 1 - \cos \frac{\pi}{2l} x \right). \quad (43)$$

Here,  $p_{\text{data}}$  denotes the pressure data at  $x = l$ . Equation (43) incorporates the value of  $p$  at  $x = l$  as a hard constraint when performing an inverse analysis to infer the vocal-fold state from speech signals. In the forward analysis,  $p_{\text{data}} = \tilde{p}$ ; thus,  $p = \tilde{p}$ . Using the obtained  $p$  together with the outputs  $x_1$  and  $x_2$  from the vocal-fold network,  $u_g$  is calculated using Eq. (15). Subsequently, based on the obtained  $u_g$ , the volume velocity  $u$  inside the vocal tract is computed as

$$u = \tilde{u} \sin \frac{\pi}{2l} x + u_g \left( 1 - \sin \frac{\pi}{2l} x \right). \quad (44)$$

This equation ensures that  $u = u_g$  at  $x = 0$ , thereby achieving coupling between glottal flow variations and vocal-tract acoustics as a hard constraint. Equation (44) corresponds to the hard-constraint method that uses distance functions to enforce Dirichlet boundary conditions [44], [45]. This approach can improve training performance because no additional loss terms are required.

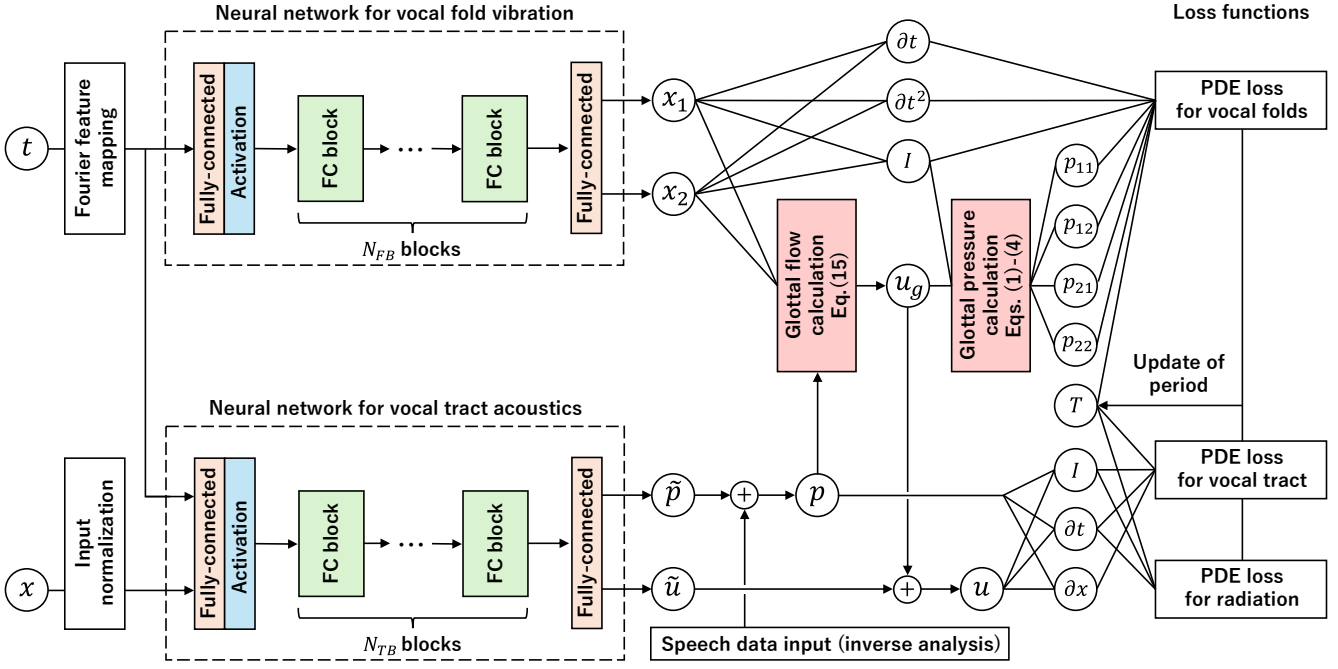


Fig. 2. Proposed PINN architecture for speech production. The upper network predicts the vocal-fold displacements, while the lower network predicts the sound pressure and volume velocity in the vocal tract. Coupled analysis is achieved by exchanging the pressure and volume velocity at  $x = 0$  between the two networks during the loss function calculation.

#### D. Differentiable Approximation Function for Glottal Closure

Glottal closure introduces nondifferentiable points into the governing equations of the vocal folds. Furthermore, at closure, Eqs. (11)–(14) yield a zero glottal area, while in Eqs. (23)–(26), the forces  $f_1$  and  $f_2$  become constants. Consequently, the time derivatives of these terms are zero, leading to vanishing gradients and preventing learning based on the backpropagation algorithm [25]. This section describes the differentiable approximation function introduced to address the learning difficulties in PINNs arising from glottal closure.

From Eqs. (11)–(14), the glottal area can be expressed as

$$A_{g,j} = \max(0, 2l_g x_{h,j}), \quad (45)$$

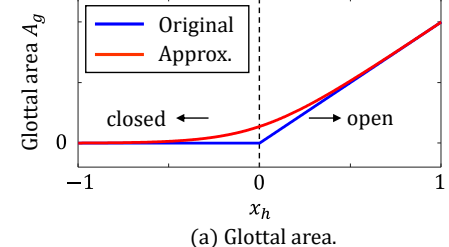
where

$$x_{h,j} = x_j - x_{\min,j}. \quad (46)$$

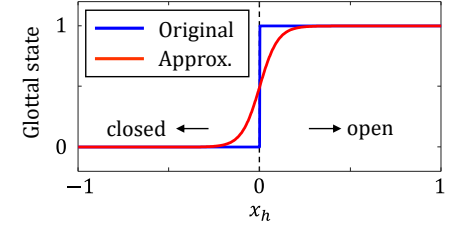
A schematic representation of Eq. (45) is indicated by the blue curve in Fig. 3(a). The derivative is discontinuous at the glottal closure point, and that the gradient vanishes for  $x_j \leq x_{\min,j}$ . To overcome this issue, in this study, the glottal area was computed using the differentiable softplus function [46] as

$$A_{g,j} = 2l_g \frac{\log(1 + e^{\beta_{A_g} x_{h,j}})}{\beta_{A_g}}, \quad (47)$$

where  $\beta_{A_g}$  denotes the smoothing coefficient. Eq. (47) is represented by the red curve in Fig. 3(a). Because the derivative remains continuous at the glottal closure point and nonzero gradients exist even for  $x_j \leq x_{\min,j}$ , training becomes feasible within the PINN framework. The use of this approximation function is consistent with the approach previously employed to analyze vocal-fold vibrations using the shooting method [7].



(a) Glottal area.



(b) Glottal state (1 = open, 0 = closed).

Fig. 3. Function approximation using differentiable functions. (a) Approximation of glottal area represented by Eq. (47). (b) Approximation of step function represented by Eq. (52).

Similarly, a differentiable approximation function was applied to the forces acting on the vocal folds. From Eqs. (23)–(26), the forces can be expressed as

$$f_1 = H(x_{h1})H(x_{h2})l_g d_1 p_1 + (1 - H(x_{h1})H(x_{h2}))l_g d_1 p_s, \quad (48)$$

$$f_2 = H(x_{h1})H(x_{h2})l_g d_2 p_2 + H(x_{h1})(1 - H(x_{h2}))l_g d_2 p_s, \quad (49)$$

where  $H$  denotes the unit-step function for the glottal state.

In this study, the step function was replaced with a sigmoid function  $\sigma$  [47], and the force  $f$  was computed as

$$f_1 = \sigma(x_{h1})\sigma(x_{h2})l_g d_1 p_1 + (1 - \sigma(x_{h1})\sigma(x_{h2}))l_g d_1 p_s, \quad (50)$$

$$f_2 = \sigma(x_{h1})\sigma(x_{h2})l_g d_2 p_2 + \sigma(x_{h1})(1 - \sigma(x_{h2}))l_g d_2 p_s, \quad (51)$$

where

$$\sigma(x) = \frac{1}{1 + e^{-\beta_f x}}, \quad (52)$$

and  $\beta_f$  is the smoothing coefficient for the forces acting on the vocal folds. A schematic comparison of the step function and the sigmoid function is shown in Fig. 3(b).

In addition, to stabilize training, the  $R_\gamma$  term in Eq. (18) is computed using the softplus function:

$$R_\gamma = -\frac{\log(1 + e^{\beta_p(p_s - p_0)})}{\beta_p}, \quad (53)$$

where  $\beta_p$  is a smoothing coefficient related to the pressure. Equation (53) is based on the assumption that  $p_s > p_0$ , that is, no backflow occurs in the glottal flow [1], [48], thereby preventing convergence to inappropriate solutions during training.

#### E. Time Scaling for Unknown Period

Limiting the simulation time to a short duration is desirable because it alleviates spectral bias [28] and enables PINNs to analyze higher-frequency components. Therefore, in this study, similar to the shooting method, only one period of vocal-fold vibration was analyzed. However, because the self-oscillation period  $T$  of the vocal folds is generally unknown, the governing equations cannot be correctly evaluated. This section describes a method for determining the period  $T$  through learning, using time scaling for unknown periods.

As shown in Eq. (41), the time  $t$  is normalized to the range  $[-1, 1]$  in the input layer of the neural network. Using the normalized time  $t^*$ , the time derivative in the governing equations can be expressed as

$$\frac{\partial}{\partial t} = \frac{2}{T} \frac{\partial}{\partial t^*}. \quad (54)$$

In the proposed method, period  $T$  is treated as a trainable parameter of the neural network. This allows the simultaneous identification of period  $T$  during the training process for the vocal-fold–vocal-tract simulation without modifying the collocation points of the input.

#### F. Loss Functions

In the proposed method, three loss functions were used: those corresponding to vocal-fold vibration, vocal-tract acoustics, and acoustic radiation. First, the loss function for vocal-fold vibration is defined based on Eqs. (21) and (22), as follows:

$$\mathcal{L}_{f1} = \frac{1}{N_f} \sum_{i=1}^{N_f} \{m_1 \ddot{x}_{1,i} + c_1 \dot{x}_{1,i} + s_{1,i} + k_c(x_{1i} - x_{2,i}) - f_{1,i}\}^2, \quad (55)$$

$$\mathcal{L}_{f2} = \frac{1}{N_f} \sum_{i=1}^{N_f} \{m_2 \ddot{x}_{2,i} + c_2 \dot{x}_{2,i} + s_{2,i} + k_c(x_{2,i} - x_{1,i}) - f_{2,i}\}^2, \quad (56)$$

where  $i$  denotes the collocation point, and  $N_f$  is the number of collocation points. Next, the loss function for the vocal-tract acoustics was defined based on Eqs. (29) and (30) as follows:

$$\mathcal{L}_{t1} = \frac{1}{N_t} \sum_{i=1}^{N_t} \left( \frac{\partial u_i}{\partial x_i} + G_i p_i + \frac{A_i}{K} \frac{\partial p_i}{\partial t_i} \right)^2, \quad (57)$$

$$\mathcal{L}_{t2} = \frac{1}{N_t} \sum_{i=1}^{N_t} \left( \frac{\partial p_i}{\partial x_i} + R_i u_i + \frac{\rho}{A_i} \frac{\partial u_i}{\partial t_i} \right)^2. \quad (58)$$

Finally, the loss function for the acoustic radiation is defined based on Eq.(37) as

$$\mathcal{L}_r = \frac{1}{N_r} \sum_{i=1}^{N_r} \left( L_r \frac{du_{l,i}}{dt_i} - p_{l,i} - \frac{L_r}{R_r} \frac{dp_{l,i}}{dt_i} \right)^2. \quad (59)$$

The total loss function of the network is given by:

$$\mathcal{L}_{all} = \lambda_f (\mathcal{L}_{f1} + \mathcal{L}_{f2}) + \lambda_{t1} \mathcal{L}_{t1} + \lambda_{t2} \mathcal{L}_{t2} + \lambda_r \mathcal{L}_r, \quad (60)$$

where  $\lambda$  denotes the weight of the loss term. The optimization problem for the proposed method is formulated as:

$$\min_{\Theta, T} \mathcal{L}_{all}(\Theta, T), \quad (61)$$

where  $\Theta$  denotes the set of trainable network parameters. By minimizing  $\mathcal{L}_{all}$  using the Adam optimizer [49], both the oscillation period  $T$  and the solutions of the governing equations are obtained.

#### G. Implementation

The proposed method was implemented using the deep-learning toolbox in MATLAB (MathWorks, USA), and a custom training loop was coded using a `dlfeval` function. The `sobolset` function from the Statistics and Machine Learning Toolbox was used to generate the  $x$  and  $t$  datasets. The networks were trained on a GPU using the Parallel Computing Toolbox. Network training and inference were conducted on a workstation equipped with an Intel Core Ultra 9 285K CPU (Intel, USA) and an NVIDIA RTX PRO 6000 Blackwell Workstation Edition GPU (NVIDIA, USA). The system has 256 GB of main memory and 96 GB of video memory.

## IV. VALIDATION OF PROPOSED METHOD

This section presents the forward and inverse analyses to verify the proposed PINN's validity.

#### A. Analysis Conditions for Forward Analysis

The performance of the proposed method in the forward analysis was verified through vowel synthesis simulations for /a/ and /u/. The vocal-tract shapes were based on the vowel configurations reported by Arai [5] and were interpolated using the Piecewise Cubic Hermite Interpolating Polynomial (PCHIP) method [50], [51]. The resulting cross-sectional areas of the vocal tract are shown in Fig. 4. The physical parameters

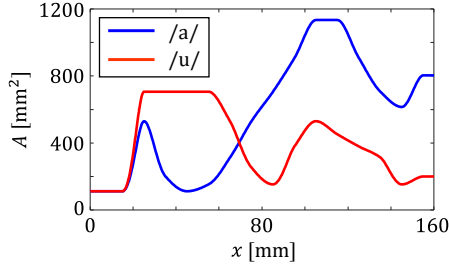


Fig. 4. Vocal-tract cross-sectional area functions. In this study, the shapes of /a/ and /u/ reported by Arai [5] were interpolated using PCHIP method [50], [51].

TABLE I  
PHYSICAL PARAMETERS.

Parameter	Value
Subglottal pressure $p_s$	785 Pa (8 cmH <sub>2</sub> O)
Vocal-fold masses $m_1, m_2$	$1.25 \times 10^{-4}, 0.25 \times 10^{-4}$ kg
Linear spring constants $k_1, k_2, k_c$	80, 8, 25 N/m
Damping coefficients $c_1, c_2$	0.020, 0.017 N · s/m
Nonlinear spring constants $\eta_{k1}, \eta_{k2}$	$1.0 \times 10^6, 1.0 \times 10^6$ m <sup>-2</sup>
Linear collision springs $h_1, h_2$	240, 24 N/m
Nonlinear collision springs $\eta_{h1}, \eta_{h2}$	$5.0 \times 10^6, 5.0 \times 10^6$ m <sup>-2</sup>
Collision position $x_{\min 1}, x_{\min 2}$	$-1.79 \times 10^{-4}$ m
Vocal-fold thicknesses $d_1, d_2$	$2.5 \times 10^{-3}, 0.5 \times 10^{-3}$ m
Vocal-fold length $l_g$	$1.4 \times 10^{-2}$ m
Air density $\rho$	1.20 kg/m <sup>3</sup>
Bulk modulus $K$	$1.39 \times 10^5$ Pa
Speed of sound $c$	340 m/s
Viscosity of air $\mu$	$1.9 \times 10^{-5}$ Pa · s
Specific heat ratio of air $\eta_{\text{air}}$	1.40
Thermal conductivity of air $\lambda_{\text{air}}$	$2.41 \times 10^{-2}$ W/(m · K)
Specific heat for const. pressure $c_p$	$1.01 \times 10^3$ J/(kg · K)
Multiplicative factor for loss $\alpha_R, \alpha_G$	25, 1
Angular frequency for loss $\omega_c$	942 rad/s (150 Hz)
Vocal-tract length $l$	0.16 m

used in the simulations are listed in Table I. The vocal-fold mechanical parameters were taken from the values reported by Ishizaka and Flanagan [1]. Because the oscillation period was unknown prior to the analysis, the initial period for the PINN was set to a value with a 20% error relative to the period obtained using the conventional method described later.

The number of nodes in each fully connected layer was set to 200. The number of FC blocks was  $N_{FB} = 3$  for the vocal-fold network and  $N_{TB} = 5$  for the vocal-tract network. The numbers of collocation points were  $N_f = 60,000$ ,  $N_t = 500$ , and  $N_r = 500$ , and the training data were divided into 12 mini-batches. The weighting coefficients of the loss functions were determined based on the curve-fitting approach for PINN outputs that we employed previously [52], resulting in  $\lambda_f = 3.50 \times 10^9$ ,  $\lambda_{t1} = 2.72 \times 10^{19}$ ,  $\lambda_{t2} = 1.01 \times 10^7$ , and  $\lambda_r = 1.00 \times 10^{10}$ . The learning rate of the Adam optimizer is scheduled as

$$\lambda_{\text{Adam}} = \frac{\lambda_{\text{init}}}{1 + \beta_{\text{Adam}} i_t}, \quad (62)$$

where  $\lambda_{\text{init}}$  denotes the initial learning rate,  $\beta_{\text{Adam}}$  is the decay rate, and  $i_t$  is the iteration index. In this analysis,  $\lambda_{\text{init}} = 6.25 \times 10^{-4}$  and  $\beta_{\text{Adam}} = 1.25 \times 10^{-4}$  were used.

For a performance comparison, we also conducted an analysis using a conventional method consisting of a vocal-

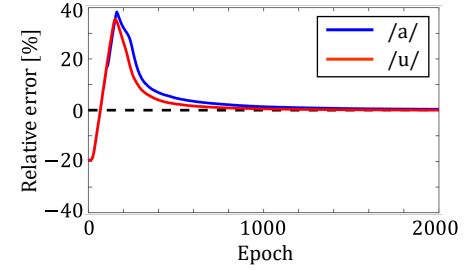


Fig. 5. Epoch-wise variation of relative error of the period  $T$  estimated by proposed method with respect to the reference value. It can be seen that, starting from an initial error of 20%, the estimated period converges to the true value after approximately 2,000 epochs.

fold model implemented with the fourth-order Runge–Kutta (RK4) scheme and a vocal-tract model implemented with the finite-difference method (FDM). The step sizes were  $\Delta x = 1.0 \times 10^{-4}$  m and  $\Delta t = 5.88 \times 10^{-8}$  s, and the forward-time, centered-space (FTCS) scheme was used for the time evolution in the FDM.

### B. Results of Forward Analysis

Figure 5 shows the evolution of the predicted period  $T$  over training epochs. In Fig. 5, the period obtained by the conventional method is considered the reference (true) value, and the relative error of the PINN prediction against this value is plotted. Starting from an initial error of 20%, the predicted period converged close to the true value after approximately 2,000 epochs. In the present simulations, after 20,000 epochs, the identified periods were  $T = 5.17 \times 10^{-3}$  s for /a/ and  $T = 5.44 \times 10^{-3}$  s for /u/, corresponding to errors of 0.14% and 0.18%, respectively, relative to the reference values.

Figure 6 shows the mass-point displacements of the vocal folds and the glottal volume velocity after 20,000 epochs of training. To illustrate periodicity, two consecutive cycles of each waveform are displayed along the time axis. For both /a/ and /u/, the results obtained using the proposed PINN agreed well with those obtained using the conventional method.

Figure 7 shows the acoustic pressure distributions in the vocal tract after 20,000 training iterations. The two columns on the left show the pressure fields obtained by the conventional method and proposed PINN, respectively, which are in close agreement. The plots on the right show the differences between the pressure fields obtained using the two methods. Although some localized discrepancies can be observed (likely due to spectral bias [28]), the results are consistent over most of the spatial domain.

Figure 8 shows the acoustic pressure waveform at  $x = l$  corresponding to the synthesized speech waveform. The results obtained using the proposed PINN closely match those obtained using the conventional method. Figure 8(b) shows the frequency spectrum of the pressure waveform at  $x = l$  obtained using the PINN. From the spectral envelope estimated via linear predictive coding (LPC) [53], clear formant structures are visible. The formant frequencies were  $F_1 = 733$  Hz and  $F_2 = 1291$  Hz for vowel /a/, and  $F_1 = 325$  Hz and

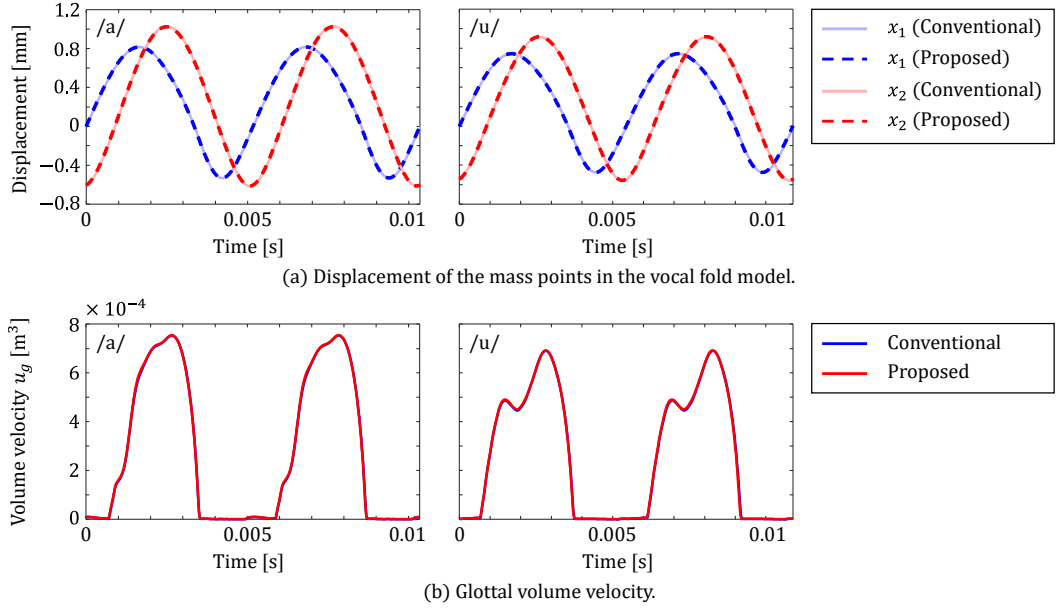


Fig. 6. Vocal-fold motion and glottal flow obtained from the forward analysis. The results obtained by the proposed PINN are in good agreement with those from the conventional method.

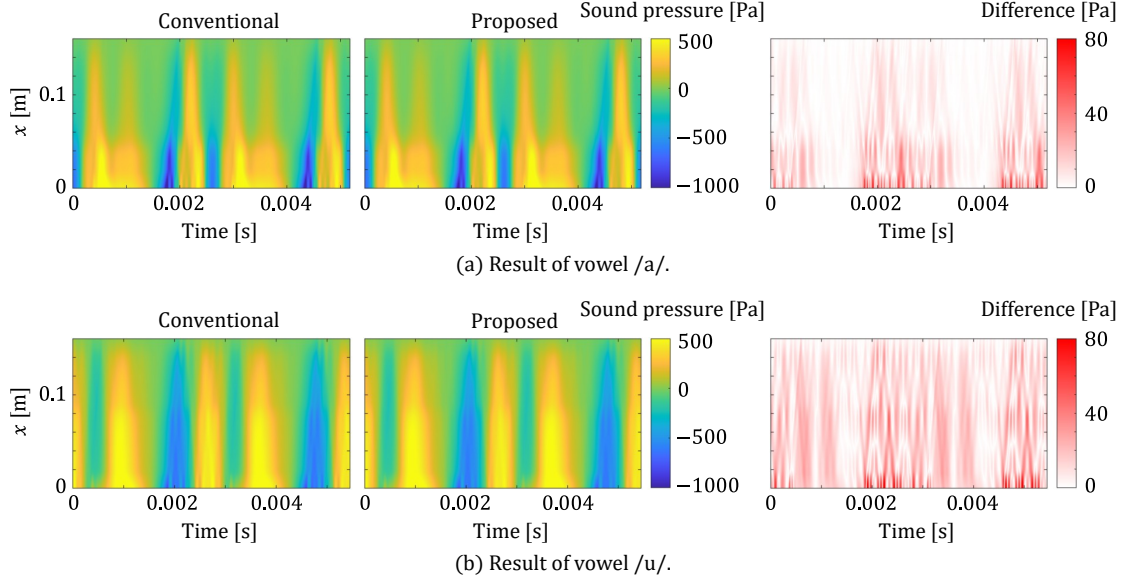


Fig. 7. Sound pressure waveform inside vocal tract obtained from the forward analysis. The results obtained by the proposed PINN agree well with those from the conventional method, although some regions show locally larger discrepancies, which are considered to be caused by spectral bias [28].

$F_2 = 561$  Hz for vowel /u/, which are close to the typical formant frequencies observed in human speech [54].

### C. Analysis Conditions for Inverse Analysis

The applicability of the proposed method to inverse analysis was demonstrated by simultaneously estimating the glottal flow  $u_g$ , vocal-fold vibration waveforms, and subglottal pressure  $p_s$  from speech waveform data. To perform the inverse analysis, the sound pressure waveform at  $x = l$  is provided to the PINN as the boundary condition. As described in Section III-C, the proposed network allows any acoustic pressure waveform data to be assigned as  $p_{\text{data}}$  in Eq. (43), thereby

enforcing the sound pressure at  $x = l$  as a hard constraint. The speech waveform used for this analysis was the vowel /a/ generated by the conventional method, identical to the “conventional” waveform in Fig 8(a). The physical parameters were the same as those used in the forward analysis (Table I), and the vocal-tract shape and vocal-fold parameters were assumed to be known.

Two minor modifications were made to the network for inverse analysis. The first concerns unknown variables. Because the oscillation period  $T$  of the speech waveform is known,  $T$  is treated as a known constant, whereas the subglottal pressure  $p_s$  is unknown and treated as a trainable parameter of the

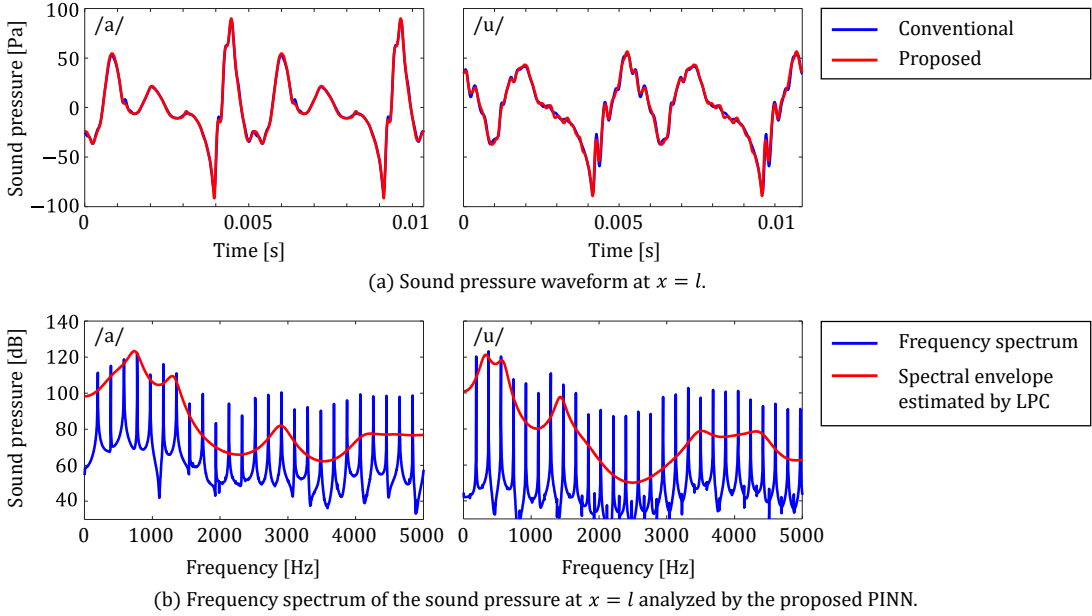


Fig. 8. Sound pressure waveform at  $x = l$ , corresponding to speech waveform. The results obtained by proposed PINN agree well with those from the conventional method. The envelope of frequency spectrum shows distinct formant peaks.

network. Accordingly, the optimization problem is formulated as:

$$\min_{\Theta, p_s} \mathcal{L}_{\text{all}}(\Theta, p_s). \quad (63)$$

The second modification concerns the weighting of loss functions. To achieve faster curve fitting at  $x = l$ , the weighting coefficient of the loss function associated with the radiation boundary at  $x = l$  was set to ten times that of the forward analysis. All other aspects of the network architecture were identical to those described in Section IV-A for the forward analysis.

#### D. Results of Inverse Analysis

Figure 9 shows the evolution of the estimated subglottal pressure  $p_s$  over training epochs. In this analysis, the result obtained by the conventional coupled analysis using the RK4 and FDM methods was used as a reference value. Fig. 9 plots the relative error of the PINN estimation with respect to this reference. Starting from an initial error of 20%, the estimated value converged sufficiently close to the reference value after approximately 2,000 epochs. After 20,000 epochs, the estimated  $p_s$  was 783.6 Pa, corresponding to a relative error of only 0.13% compared to the reference value.

Figure 10 shows the motion of the vocal-fold mass points and the estimated glottal volume velocity after 20,000 epochs of training. Both waveforms were in close agreement with the reference results, demonstrating that the proposed method can accurately estimate the state of the vocal folds.

The total computation time for 20,000 training epochs was 5 h and 35 min, indicating that reducing the computation time remains a challenge. Nevertheless, as described in Sections III and IV-C, the proposed method enables inverse analysis using nearly the same network structure as that used for forward analysis without requiring a separate, complex algorithm. In

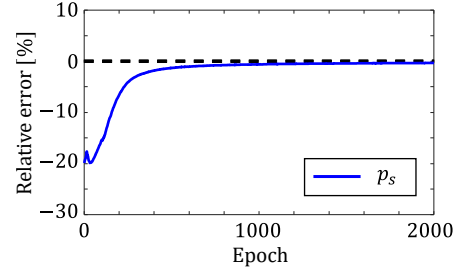


Fig. 9. Epoch-wise variation of relative error of subglottal pressure  $p_s$  estimated by PINN with respect to the reference value. It can be seen that, starting from an initial error of 20%, the estimated value converges to the true value after approximately 2,000 epochs of training.

addition, the method retains the advantages of PINNs, such as mesh-free implementation using automatic differentiation and the natural incorporation of nonlinearities. Therefore, the proposed approach is expected to be applicable to a wide range of inverse problems in speech analysis.

## V. CONCLUSION

We proposed a physics-informed neural network (PINN) capable of performing speech production analysis by coupling vocal-fold vibrations with vocal-tract resonance, and demonstrated its ability to estimate vocal-fold states from speech waveforms. The proposed PINN architecture introduces several approaches to address the challenges inherent in speech production, including a differentiable approximation function to overcome the nonlinearity associated with vocal-fold collision, a hard constraint to couple the vocal folds and vocal tract, and a time-scaling method to account for the unknown period of vocal-fold self-oscillation.

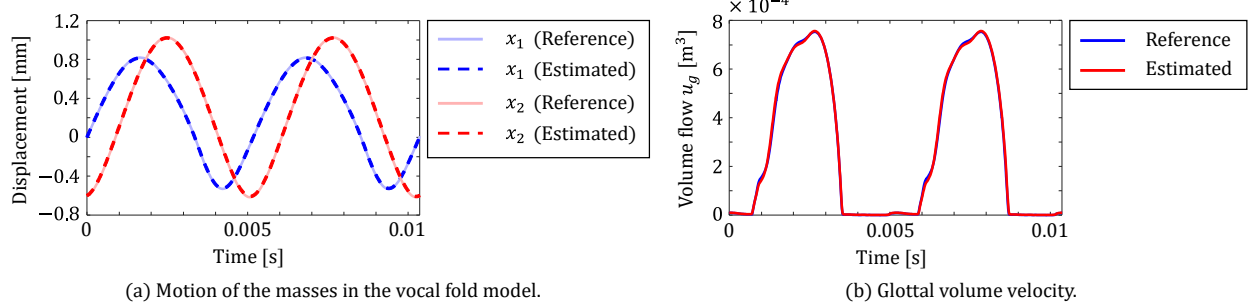


Fig. 10. Vocal-fold motion and glottal flow estimated by proposed PINN. The estimated waveforms are found to be in close agreement with the reference values.

In forward analysis, the proposed method successfully produced vocal-fold vibrations and speech waveforms that closely matched those obtained using the conventional method. In inverse analysis, by providing the speech waveform as input to the PINN, the vocal-fold motion, glottal flow, and subglottal pressure were accurately estimated, demonstrating the high performance of the proposed approach.

The proposed method offers several advantages, such as eliminating the need for complex algorithms for inverse analysis, naturally incorporating nonlinearities, and enabling mesh-free computation through automatic differentiation. Future work will focus on extending the method to two- and three-dimensional analyses and applying it to the analysis of consonants and singing voices.

#### ACKNOWLEDGMENTS

This work was supported by JSPS KAKENHI Grant Number JP 25K03137 and the Ono Charitable Trust for Acoustics.

#### REFERENCES

- [1] K. Ishizaka and J. L. Flanagan, "Synthesis of voiced sounds from a two-mass model of the vocal cords," *Bell system technical journal*, vol. 51, no. 6, pp. 1233–1268, 1972.
- [2] I. R. Titze, "The physics of small-amplitude oscillation of the vocal folds," *The Journal of Acoustical Society of America*, vol. 83, no. 4, pp. 1536–1552, 1988.
- [3] J. R. Lechien, S. Saussez, B. Harmegnies, C. Finck, and J. A. Burns, "Laryngopharyngeal reflux and voice disorders: a multifactorial model of etiology and pathophysiology," *Journal of voice*, vol. 31, no. 6, pp. 733–752, 2017.
- [4] P. Gómez-Vilda, R. Fernández-Baillo, A. Nieto, F. Díaz, F. J. Fernández-Camacho, V. Rodelar, A. Álvarez, and R. Martínez, "Evaluation of voice pathology based on the estimation of vocal fold biomechanical parameters," *Journal of Voice*, vol. 21, no. 4, pp. 450–476, 2007.
- [5] T. Arai, "Education system in acoustics of speech production using physical models of the human vocal tract," *Acoustical science and technology*, vol. 28, no. 3, pp. 190–201, 2007.
- [6] R. B. Monsen, A. M. Engebretson, and N. R. Vemula, "Indirect assessment of the contribution of subglottal air pressure and vocal-fold tension to changes of fundamental frequency in english," *The Journal of the Acoustical Society of America*, vol. 64, no. 1, pp. 65–80, 1978.
- [7] K. Yokota, S. Ishikawa, K. Takezaki, Y. Koba, and S. Kijimoto, "Numerical analysis and physical consideration of vocal fold vibration by modal analysis," *Journal of Sound and Vibration*, vol. 514, p. 116442, 2021.
- [8] R. Mittal, X. Zheng, R. Bhardwaj, J. H. Seo, Q. Xue, and S. Bielamowicz, "Toward a simulation-based tool for the treatment of vocal fold paralysis," *Frontiers in physiology*, vol. 2, p. 19, 2011.
- [9] T. Tran, J. Perry, S. Blemker, and K. Mason, "Simulation of velopharyngeal biomechanics identifies differences in sphincter pharyngoplasty outcomes: A matched case-control study," *The Cleft Palate Craniofacial Journal*, vol. 61, no. 2, pp. 339–349, 2024.
- [10] K. Yokota, S. Ishikawa, Y. Koba, S. Kijimoto, and S. Sugiki, "Inverse analysis of vocal sound source using an analytical model of the vocal tract," *Applied Acoustics*, vol. 150, pp. 89–103, 2019.
- [11] J. Schroeter and M. M. Sondhi, "Techniques for estimating vocal-tract shapes from the speech signal," *IEEE Transactions on Speech and Audio Processing*, vol. 2, no. 1, pp. 133–150, 1994.
- [12] P. Alku, "Glottal inverse filtering analysis of human voice production—a review of estimation and parameterization methods of the glottal excitation and their applications," *Sadhana*, vol. 36, no. 5, pp. 623–650, 2011.
- [13] G. Fant, *Acoustic theory of speech production: with calculations based on X-ray studies of Russian articulations*. Walter de Gruyter, 1971, no. 2.
- [14] W. Zhao and R. Singh, "Deriving vocal fold oscillation information from recorded voice signals using models of phonation," *Entropy*, vol. 25, no. 7, p. 1039, 2023.
- [15] R. Blandin, M. Arnela, S. Félix, J.-B. Doc, and P. Birkholz, "Efficient 3d acoustic simulation of the vocal tract by combining the multimodal method and finite elements," *IEEE Access*, vol. 10, pp. 69 922–69 938, 2022.
- [16] M. Raissi, P. Perdikaris, and G. E. Karniadakis, "Physics-informed neural networks: A deep learning framework for solving forward and inverse problems involving nonlinear partial differential equations," *Journal of Computational physics*, vol. 378, pp. 686–707, 2019.
- [17] S. Cuomo, V. S. Di Cola, F. Giampaolo, G. Rozza, M. Raissi, and F. Piccialli, "Scientific machine learning through physics-informed neural networks: Where we are and what's next," *Journal of Scientific Computing*, vol. 92, no. 3, p. 88, 2022.
- [18] A. Farea, O. Yli-Harja, and F. Emmert-Streib, "Understanding physics-informed neural networks: Techniques, applications, trends, and challenges," *AI*, vol. 5, no. 3, pp. 1534–1557, 2024.
- [19] X. Jiang, D. Wang, Q. Fan, M. Zhang, C. Lu, and A. P. T. Lau, "Physics-informed neural network for nonlinear dynamics in fiber optics," *Laser & Photonics Reviews*, vol. 16, no. 9, p. 2100483, 2022.
- [20] J. D. Schmid, P. Bauerschmidt, C. Gurbuz, M. Eser, and S. Marburg, "Physics-informed neural networks for acoustic boundary admittance estimation," *Mechanical Systems and Signal Processing*, vol. 215, p. 111405, 2024.
- [21] X. Karakontantis, D. Caviedes-Nozal, A. Richard, and E. Fernandez-Grande, "Room impulse response reconstruction with physics-informed deep learning," *The Journal of the Acoustical Society of America*, vol. 155, no. 2, pp. 1048–1059, 2024.
- [22] X. Chen, F. Ma, A. Bastine, P. Samarasinghe, and H. Sun, "Sound field estimation around a rigid sphere with physics-informed neural network," in *2023 Asia Pacific Signal and Information Processing Association Annual Summit and Conference (APSIPA ASC)*. IEEE, 2023, pp. 1984–1989.
- [23] K. Yokota, M. Ogura, and M. Abe, "Synthesis of voiced sounds using physics-informed neural networks," *Acoustical Science and Technology*, vol. 45, no. 6, pp. 333–336, 2024.
- [24] K. Hornik, "Approximation capabilities of multilayer feedforward networks," *Neural networks*, vol. 4, no. 2, pp. 251–257, 1991.

[25] D. E. Rumelhart, G. E. Hinton, and R. J. Williams, "Learning representations by back-propagating errors," *nature*, vol. 323, no. 6088, pp. 533–536, 1986.

[26] L. Liu, S. Liu, H. Xie, F. Xiong, T. Yu, M. Xiao, L. Liu, and H. Yong, "Discontinuity computing using physics-informed neural networks," *Journal of Scientific Computing*, vol. 98, no. 1, p. 22, 2024.

[27] A. Chaumet and J. Giesselmann, "Improving weak pinns for hyperbolic conservation laws: Dual norm computation, boundary conditions and systems," *arXiv preprint arXiv:2211.12393*, 2022.

[28] S. Wang, X. Yu, and P. Perdikaris, "When and why pinns fail to train: A neural tangent kernel perspective," *Journal of Computational Physics*, vol. 449, p. 110768, 2022.

[29] H. Sethi, D. Pan, P. Dimitrov, J. Shragge, G. Roth, and K. Hester, "Hard enforcement of physics-informed neural network solutions of acoustic wave propagation," *Computational geosciences*, vol. 27, no. 5, pp. 737–751, 2023.

[30] J. C. Wong, A. Gupta, C. C. Ooi, P.-H. Chiu, J. Liu, and Y.-S. Ong, "Evolutionary optimization of physics-informed neural networks: Survey and prospects," *arXiv preprint arXiv:2501.06572*, 2025.

[31] M. R. Osborne, "On shooting methods for boundary value problems," *Journal of mathematical analysis and applications*, vol. 27, no. 2, pp. 417–433, 1969.

[32] J. L. Flanagan, *Speech analysis synthesis and perception*. Springer Science & Business Media, 2013, vol. 3.

[33] J. J. Jiang and Y. Zhang, "Chaotic vibration induced by turbulent noise in a two-mass model of vocal folds," *The Journal of the Acoustical Society of America*, vol. 112, no. 5, pp. 2127–2133, 2002.

[34] Y. Zhang, J. Jiang, and D. A. Rahn, "Studying vocal fold vibrations in parkinson's disease with a nonlinear model," *Chaos: An Interdisciplinary Journal of Nonlinear Science*, vol. 15, no. 3, 2005.

[35] A. P. Pinheiro and G. Kerschen, "Vibrational dynamics of vocal folds using nonlinear normal modes," *Medical Engineering & Physics*, vol. 35, no. 8, pp. 1079–1088, 2013.

[36] J. C. Lucero, "Dynamics of the two-mass model of the vocal folds: Equilibria, bifurcations, and oscillation region," *The Journal of the Acoustical Society of America*, vol. 94, no. 6, pp. 3104–3111, 1993.

[37] K. Yokota, T. Kurahashi, and M. Abe, "Physics-informed neural network for acoustic resonance analysis in a one-dimensional acoustic tube," *The Journal of the Acoustical Society of America*, vol. 156, no. 1, pp. 30–43, 2024.

[38] L. Ziyin, T. Hartwig, and M. Ueda, "Neural networks fail to learn periodic functions and how to fix it," *Advances in Neural Information Processing Systems*, vol. 33, pp. 1583–1594, 2020.

[39] L. Lu, R. Pestourie, W. Yao, Z. Wang, F. Verdugo, and S. G. Johnson, "Physics-informed neural networks with hard constraints for inverse design," *SIAM Journal on Scientific Computing*, vol. 43, no. 6, pp. B1105–B1132, 2021.

[40] C. Song and Y. Wang, "Simulating seismic multifrequency wavefields with the fourier feature physics-informed neural network," *Geophysical Journal International*, vol. 232, no. 3, pp. 1503–1514, 2023.

[41] O. Sallam and M. Fürth, "On the use of fourier features-physics informed neural networks (ff-pinn) for forward and inverse fluid mechanics problems," *Proceedings of the Institution of Mechanical Engineers, Part M: Journal of Engineering for the Maritime Environment*, vol. 237, no. 4, pp. 846–866, 2023.

[42] S. W. Kim, E. Kwak, J.-H. Kim, K.-Y. Oh, and S. Lee, "Modeling and prediction of lithium-ion battery thermal runaway via multiphysics-informed neural network," *Journal of Energy Storage*, vol. 60, p. 106654, 2023.

[43] Z. Wu, H. Wang, C. He, B. Zhang, T. Xu, and Q. Chen, "The application of physics-informed machine learning in multiphysics modeling in chemical engineering," *Industrial & Engineering Chemistry Research*, vol. 62, no. 44, pp. 18 178–18 204, 2023.

[44] N. Sukumar and A. Srivastava, "Exact imposition of boundary conditions with distance functions in physics-informed deep neural networks," *Computer Methods in Applied Mechanics and Engineering*, vol. 389, p. 114333, 2022.

[45] S. Berrone, C. Canuto, M. Pintore, and N. Sukumar, "Enforcing dirichlet boundary conditions in physics-informed neural networks and variational physics-informed neural networks," *Heliyon*, vol. 9, no. 8, 2023.

[46] C. Dugas, Y. Bengio, F. Bélisle, C. Nadeau, and R. Garcia, "Incorporating second-order functional knowledge for better option pricing," *Advances in neural information processing systems*, vol. 13, 2000.

[47] D. E. Rumelhart, G. E. Hinton, and R. J. Williams, "Learning representations by back-propagating errors," *nature*, vol. 323, no. 6088, pp. 533–536, 1986.

[48] M. Krane, M. Barry, and T. Wei, "Unsteady behavior of flow in a scaled-up vocal folds model," *The Journal of the Acoustical Society of America*, vol. 122, no. 6, pp. 3659–3670, 2007.

[49] D. P. Kingma, "Adam: A method for stochastic optimization," *arXiv preprint arXiv:1412.6980*, 2014.

[50] F. N. Fritsch and R. E. Carlson, "Monotone piecewise cubic interpolation," *SIAM Journal on Numerical Analysis*, vol. 17, no. 2, pp. 238–246, 1980.

[51] F. N. Fritsch and J. Butland, "A method for constructing local monotone piecewise cubic interpolants," *SIAM journal on scientific and statistical computing*, vol. 5, no. 2, pp. 300–304, 1984.

[52] K. Yokota, M. Ogura, and M. Abe, "Identification of physical properties in acoustic tubes using physics-informed neural networks," *Mechanical Engineering Journal*, vol. 11, no. 5, pp. 24–00 228, 2024.

[53] F. Itakura, "A statistical method for estimation of speech spectral density and formant frequencies," *Electro. Comm. Japan, A*, vol. 53, no. 1, pp. 36–43, 1970.

[54] A. T. Neel, "Vowel space characteristics and vowel identification accuracy," *Journal of Speech, Language, and Hearing Research*, vol. 51, no. 3, pp. 574–585, 2008.